



---

# Study of Atomic Hydrogen in Brazilian Rubellite by EPR Spectroscopy

S. Isotani<sup>1\*</sup> and W. M. Pontuschka<sup>1</sup>

<sup>1</sup>Institute of Physics of University of São Paulo, São Paulo, SP, Brazil.

### Authors' contributions

*This work was carried out in collaboration between the authors. All authors read and approved the final manuscript.*

Research Article

Received 29<sup>th</sup> March 2013  
Accepted 19<sup>th</sup> August 2013  
Published 7<sup>th</sup> October 2013

---

## ABSTRACT

**Aims:** The Electron Paramagnetic Resonance (EPR) absorption study of atomic hydrogen is an useful tool that offers perhaps the first direct experimental method to study the distribution of local ring structures in glasses and in other amorphous materials.

**Study Design:** In the present work we intend to analyze earlier data on the EPR of the atomic hydrogen in Brazilian rubellite crystal.

**Place and Duration of Study:** Institute of Physics, July 2012 to December 2012.

**Methodology:** Isothermal decay behaviors of H<sup>0</sup> centers at 353, 364, 373, 383, 393, 403, 413, 423, 433 and 443 K, for the EPR absorption line in gamma-irradiated rubellite were analyzed using a kinetic model consisting of H<sup>0</sup> confined in a cage formed on one side by the brucite octahedrons and on another side by ions of Y<sup>+</sup> (Y=Na, K). The parameters describing these defects were determined with a grid optimization method. The isochronal kinetics is simulated taking in account the heating process and the kinetic equations obtained on the basis of this model were solved using the method of Runge-Kutta.

**Results:** It is shown that the decay process consists of two exponential components, which is consistent with the two independent first order kinetics and the model of creation and annihilation of H<sup>0</sup> in cages.

**Conclusion:** Two H<sup>0</sup> centers were found with activation energies E<sub>1</sub> = (0.55 ± 0.04) eV and E<sub>2</sub> = (0.99 ± 0.04) eV.

*Keywords: Rubellite; atomic hydrogen; EPR; isothermal kinetics; isochronal kinetics.*

---

\*Corresponding author. Email: [sisotani@if.usp.br](mailto:sisotani@if.usp.br);

## 1. INTRODUCTION

A study by electron paramagnetic resonance (EPR) of the atomic hydrogen center ( $H^0$ ) in natural crystals of Brazilian rubellite (pink tourmaline),  $NaX_3Al_6B_3Si_6O_{27}(OH,F)_4$ , where X = Li, Al, Mn, Fe, submitted to  $\gamma$ -irradiation of  $^{60}Co$  source has been previously reported and a model for the mechanism of neutral hydrogen atom stabilization was proposed [1,2]. The rubellite crystals were from a Minas Gerais pegmatite source. They were of a pinkish color, with an elongated prismatic shape with a rounded triangular cross-section. The Mn and Fe impurity concentrations were found to be variable throughout the volume of the samples in the range of 8690 to 11050 ppm and 250 to 700 ppm, respectively [3].

To discuss the stabilization model of the  $H^0$  presented by Camargo et al. [1] the graphical description of the structure of rubellite as described by Godovikov [4] is essential. For this reason, Fig. 1 presented by Camargo et al. [1,2] is reproduced as Fig. 1 of the present report.

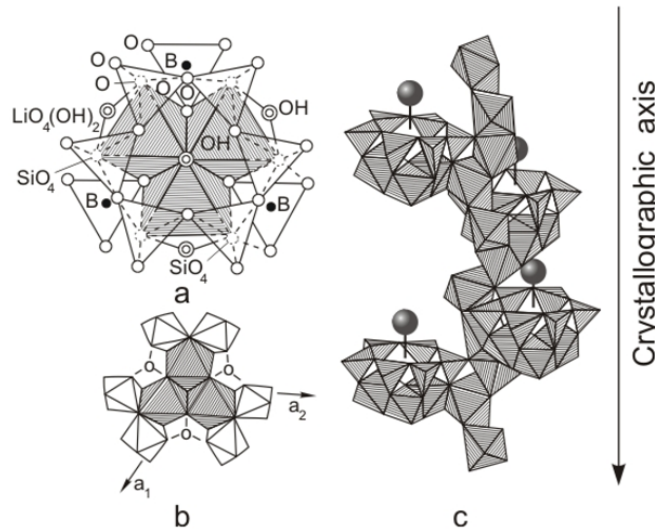


**Fig. 1. The structure of rubellite, after Buerger et al. [5]. (a) Structural grouping of antigorite, consisting of a brucite at the bottom (three octahedra of  $LiO_4(OH)_2$  and planar  $BO_3$  units) and hexagonal silicate ring at the top. (b) Bottom view of the brucite with  $AlO_5(OH)$  octahedral. (c) Helicoidal chain of antigorite units connected by means of  $AlO_5(OH)$  octahedral where the black spheres represent ions of  $Y^+$  ( $Y=Na, K$ ). This figure is a reproduction of Fig. 1 reported by Camargo et al. [1,2]**

A very strong inhomogeneous dipolar interaction is inferred from the large linewidth of 15 G, constant over the whole temperature range of 4.2 to 265 K, indicating that the atomic hydrogen fraction that can be detected by EPR interacts strongly with neighboring ions in the rubellite crystal structure.

Hydrogen is found in the hydroxyls located in positions well-defined in the rubellite unit cell [5]. The rubellite structure is composed of antigorite units like those shown in Fig. 1. The antigorite is composed of a brucite at the bottom and a ring of six  $SiO_4$  tetrahedral structural units at the middle. The brucite consists of three  $LiO_4(OH)_2$  octahedral units and  $BO_3$  planar

triangles, with an OH occupying the common vertex. The antigorite units are interconnected by  $\text{AlO}_5(\text{OH})$  octahedrons, forming a helicoidal chain. Finally, in addition to the internal OH, three more OH groups are externally bonded to the antigorite.

The brucite has a structure in the form of a cage with an  $\text{Y}^+$  ( $\text{Y}=\text{Na}, \text{K}$ ) ion enclosing the volume. A model in which  $\text{H}^0$  is stabilized at the centers of oxygen polygons belonging to B–O ring structures by van der Waals forces have been proposed [6,7]. This model was supported by analysis of the kinetics using a microscopic model and the calculation of the dispersion energy [8]. Following these findings, we will assume here that the  $\text{H}^0$  produced by decomposition of the OH occupying the common vertex is stabilized at the ring of the oxygen polygons belonging to the Si-O ring structure. The presence of a  $\text{Y}^+$  ion enclosing the brucite confines the  $\text{H}^0$  within the brucite volume. Therefore, on heating the recombination of  $\text{H}^0$  and the oxygen ion at the vertex of the brucite must follow a first order kinetics.

The measured isothermal decay kinetics indicates a fast initial decay followed by a slower decrease of the atomic hydrogen EPR signal intensity. Isochronal decay measurements presented a sequence of subsequent bumps. These decay data were attributed to the thermal decay of  $\text{H}^0$  trapped at specific stabilization sites, described on the basis of structural considerations [6]. The radiation-induced  $\text{H}^0$  were produced by the radiolysis of OH. As shown in Fig. 1a, only one hydroxyl is found inside the antigorite cage. As the radiolysis of the external hydroxyls produces  $\text{H}^0$  outside this cage, it is expected that they recombine readily at room temperature and will not be detected by EPR. Thus, the radiolysis of the OH located at the center of the hexagonal ring of  $\text{SiO}_4$  tetrahedrons, confined on one side by the brucite octahedrons and on another side by ions of  $\text{Y}^+$ , produces  $\text{H}^0$  that is stable at room temperature. The first order kinetics observed for the slower decay, together the low diffusion probability, support a model in which the atomic hydrogen produced from OH hydrolysis recombines on heating with the non-bridging oxygen ion which remained inside the brucite cage covered by the  $\text{Y}^+$  ion.

Atomic hydrogen has proven to be a useful tool, and offers perhaps the first direct experimental method for the study of local ring structure arrays in amorphous materials [6]. Thus, the purpose of this work is to analyze earlier data on the EPR of  $\text{H}^0$  in rubellite [1,2] in order to refine knowledge about  $\text{H}^0$  stabilization sites. We report the analysis of the temperature dependency of the EPR intensity, the analysis of isothermal decay using recently developed calculation method and we describe a method for the simulation of isochronal decay.

## 2. MATERIALS AND METHODS

### 2.1 The EPR Spectra

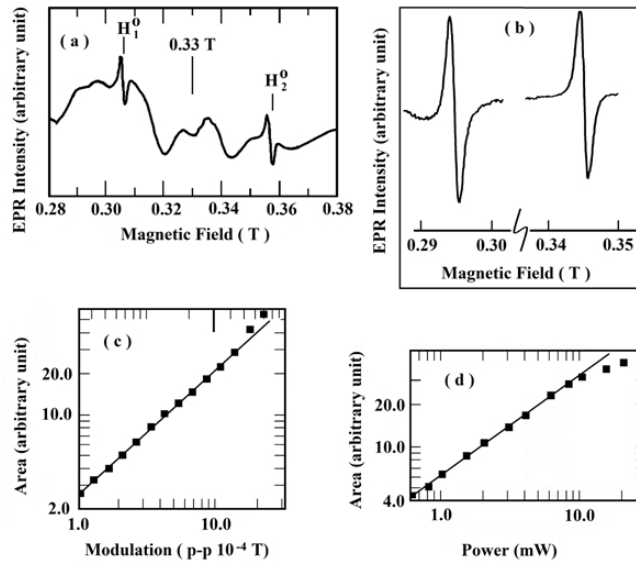
The EPR data for intensity and line shape from previous references [1,2] that are revised in the present report were collected with a homemade X-band homodyne reflection-type spectrometer. The calibration of the magnetic field was done using a RMN gaussmeter. The data used in Figs. 3 and 4 are the area under the EPR absorption lines. The area reflects the amount of spins multiplied by experimental factors. Then we retain that part reflecting the amount of spins normalizing the data for each process to their starting area.

Fig. 2a showing the EPR spectrum of rubellite presented by Camargo et al. [1,2]. The two lines of  $\text{H}^0$  have peak to peak line width of about  $15 \times 10^{-4}$  T. Fig. 2b shows the expanded

spectrum of  $H^0$ . We can observe that the line is slightly deformed suggesting the possibility that this line is composed of  $H^0$  trapped at different sites. Fig. 2c shows the relationship between magnetic field modulation and the signal height, which occur at modulation above  $10 \times 10^{-4}$  T. So we adopted the magnetic field modulation of  $5 \times 10^{-4}$  T, below the deviation from the linear relationship between the modulation amplitude and the signal height. Fig. 2d shows the relationship between the microwave power and the line saturation, which occurs at powers above 10 mW. For this reason we adopted the power of 8mW or less in measurements.

The line character of the EPR absorption line was determined following the procedure described by Alger [9]. The line character for the first line is  $(2.38 \pm 0.24)$  and for the second line is  $(2.62 \pm 0.29)$ , in units normalized to the half of the peak to peak distance. The line character for a Gaussian line is 2.5 and for a Lorentzian line is 3.8. So we see that the character of the line is very close to Gaussian.

A group of spins which interact very little with the network and has a long  $T_1$  relaxation time, provides a narrow Lorentzian shape line [10] and on the other hand if they interact with the network there occurs a superposition of these lines resulting in a broadening of its contour. One possible cause of broadening could be the interaction of  $H^0$  with the nuclear spin of  $Na^+$ . However, this interaction results in broadening of about 0.0002 T [11] which is insufficient to explain the line width. Other contributions may originate by interactions with paramagnetic ions of brucite. As these ions are distributed randomly in the solid solution, and since the line shape is dependent on the local electric field, the line shape tends to be Gaussian. The average value of the character of the line is smaller for the first line and higher for the second line relative to the expected value for the Gaussian line. This small distortion may reflect absorption by  $H^0$  trapped at different sites.



**Fig. 2. (a) EPR spectrum of rubellite; (b) expanded EPR spectrum of rubellite; (c) relationship between the area of the EPR absorption line with magnetic field modulation; (d) relationship between the area of the EPR absorption line with microwave power. All measurements have been done at 300°C**

## 2.2 Kinetics of the EPR Spectra

The isothermal decay measurements of the  $H^0$  centers in rubellite at 353, 364, 373, 383, 393, 403, 413, 423, 433 and 443 K were obtained under a flux of heated nitrogen gas heated to a constant temperature. This flux was injected into a quartz tube containing the sample, which was inserted in the EPR resonant cavity. With this procedure we kept the temperature constant during the measurements. Then the  $H^0$  signal was recorded over time at constant temperature and they can be compared to each other. The line shape remained without changes during the measurements. After a series of measurements at a constant temperature  $T_1$ , the sample was annealed at 400°C for 8 to 10 hours removing the remaining  $H^0$  which was confirmed by EPR measurements. Then the sample was irradiated again recovering the amount of  $H^0$ . The same heating process was repeated at another constant temperature  $T_2$ , and so on.

Isochronal heat treatment was performed directly in the EPR resonant cavity using a different procedure from one used in the isothermal measurements. The line shape of the EPR absorption line changes with temperature preventing comparison of intensities between lines obtained at different temperatures. Then, the sample was heated up to temperature  $T_1$ , held for 10 minutes and then lowered to 303 K for EPR measurement. In the subsequent step, the temperature was raised to a greater constant temperature  $T_2$ , held for 10 minutes and then lowered to 303 K for EPR measurement and the entire process was repeated for higher temperatures.

## 3. RESULTS AND DISCUSSION

The isothermal decay of  $H^0$  at different temperatures is shown in Fig. 3a. About 20% of the hydrogen is recombined during the initial fast decay, while the remaining portion of the curve follows a first order kinetics. It has been shown that the long-term decay follows first-order decay with activation energy of about 1 eV [1].

In the previous section it was suggested that the temperature dependence of EPR spectra are consistent with the modeled stabilization of  $H^0$  in the brucite cage enclosed by a  $Y^+$  ion that was proposed in previous report [1]. In this case the most probable kinetic model is that  $H^0$  escapes from the site of stabilization, going directly to non bridging oxygen, and the expected kinetics is of the first order.

Accordingly, the experimental isotherms shown in Fig. 3 can be readily decomposed in two exponentials, assigned respectively to non-equivalent sites of  $H^0$  stabilization centers:

$$I = a_1 \exp(-b_1 t) + a_2 \exp(-b_2 t) \quad (1)$$

where  $I$  is the intensity of the atomic hydrogen EPR line,  $t$  is the thermal decay time, and  $a_i$  and  $b_i$  are constants for each isotherm ( $i=1,2$ ). This observation shows that the main process of the kinetics is of the first order. The parameters were obtained using the grid optimization method [12,13]. The errors from the parameters due to the fitting procedure are calculated by increasing and decreasing the parameter values from the respective best-fit parameter values and adopting as the deviation from each best-fit parameter value the largest difference in magnitude between the best-fit parameter value and a parameter value giving a 20% increase in cost function [14,15]. In the calculation of parameter errors we also considered errors due to experimental error of about 5%.

The best-fit isothermal curves are shown as solid lines in Fig. 3a and the parameters are shown in Table 1.

The exponential decay rates  $b_i$  exhibit an Arrhenius type (see Figs, 3b and 3c) temperature dependence:

$$b_i = b_{0i} \exp\left(-\frac{E_i}{kT}\right) \quad (2)$$

where  $T$  is the thermal decay temperature,  $k$  the Boltzmann constant,  $E_i$  the activation energy and  $b_{0i}$  the frequency factor of the  $i$ -th decay component ( $i=1,2$ ). The least squares fit of  $b_1$  and  $b_2$  yields activation energies  $E_1 = (0.55 \pm 0.04)$  eV and  $E_2 = (0.99 \pm 0.04)$  eV, and pre-exponential factors  $b_{01} = (35.7 \pm 5.5) 10^3 \text{ s}^{-1}$  and  $b_{02} = (56.0 \pm 9.7) 10^7 \text{ s}^{-1}$ , respectively.

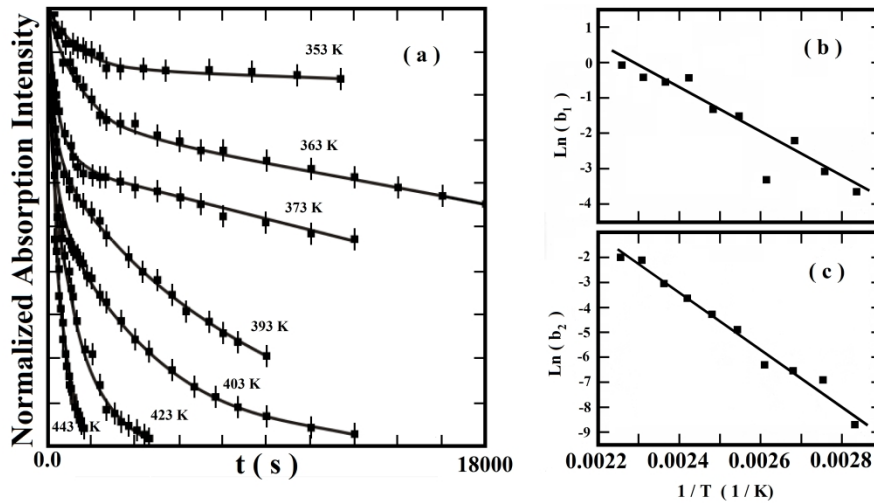


Fig. 3. (a) Plot of the isothermal decay of  $H^0$  EPR absorption intensity. Symbols ■ show the experimental results and solid lines show the best fit results; (b) Arrhenius plot of the recombination rate  $b_1$ ; (c) Arrhenius plot of the recombination rate  $b_2$

Table 1. The best-fit parameters for equation 1

T(K)	$b_1$ ( $\text{min}^{-1}$ )	$a_1$	$b_2$ ( $\text{min}^{-1}$ )	$a_2$
353	$0.0278 \pm 0.0053$	$0.0747 \pm 0.0091$	$0.00015 \pm 0.00015$	$0.925 \pm 0.010$
363	$0.0461 \pm 0.0047$	$0.0996 \pm 0.0056$	$0.00101 \pm 0.00013$	$0.9004 \pm 0.0056$
373	$0.1101 \pm 0.0081$	$0.0781 \pm 0.0031$	$0.00145 \pm 0.00016$	$0.9219 \pm 0.0031$
383	$0.03655 \pm 0.0077$	$0.098 \pm 0.013$	$0.00184 \pm 0.00031$	$0.902 \pm 0.013$
393	$0.220 \pm 0.0251$	$0.0819 \pm 0.0050$	$0.00760 \pm 0.00047$	$0.9181 \pm 0.0050$
403	$0.266 \pm 0.047$	$0.130 \pm 0.012$	$0.0140 \pm 0.0019$	$0.870 \pm 0.012$
413	$0.65 \pm 0.43$	$0.0235 \pm 0.0053$	$0.0268 \pm 0.0022$	$0.9765 \pm 0.0053$
423	$0.58 \pm 0.272$	$0.0460 \pm 0.0097$	$0.0477 \pm 0.0035$	$0.9540 \pm 0.0097$
433	$0.66 \pm 0.48$	$0.025 \pm 0.010$	$0.1217 \pm 0.0046$	$0.975 \pm 0.010$
443	$0.94 \pm 0.79$	$0.0157 \pm 0.0054$	$0.1368 \pm 0.0032$	$0.9843 \pm 0.0054$

The pre-exponential factors of the two components of the decay are quite different and the activation energies differ by a factor 2. In the analysis of the kinetic decay process of  $H^0$  in a-Si:(H,O,N) and natural beryl it has been shown that the pre exponential factor is related directly to the recombination cross section of  $H^0$  [16]. In the present case, the large difference between the pre-exponential factors means that we should expect a large difference in the recombination cross section. Here we attributed the two components of the decay processes to the recombination of  $H^0$  trapped in two cavities formed by a brucite and the ions  $Na^+$  and  $K^+$ . Therefore, we concluded that the large difference between the pre-exponential factors reveals the important effect of  $Y^+$  ions in the stabilization of  $H^0$ .

In our case the cross section of recombination can be considered the same for both sites. However as the energy of relaxation contributes exponentially to the pre exponential factor we concluded that the results presented above are consistent.

Simulation of the isochronal decay is complex because the measurements were not continuous like the isothermal decays as described in section 2.2. The simulation of this process requires solving the first order kinetic equation for each  $i$ -th process ( $i=1,2$ ) to include the steps of heating and cooling:

$$\frac{dI_i}{dt} = -b_{0i} \exp\left(-\frac{E_i}{kT}\right) I_i \quad (3)$$

where  $I_i$  is proportional to the actual concentration of hydrogen atomic centers stabilized in the  $i$ -th center,  $T$  is the applied temperature,  $b_{0i}$  is the frequency factor, and  $E_i$  the activation energy of the  $i$ -th center.

Equation (3) was solved using the Runge-Kutta method [17], taking the experimental conditions into account. The first condition is that the initial temperature of measurement of the EPR spectra is assumed to be the same  $T_{ini}$  for all data. After this measurement, the temperature of the sample was raised to  $T_{nom}$  with a heated gas flux passed around the sample holder.

As our samples are thin and the temperature change large enough, the heat conduction follows an exponential behavior given by [21]:

$$T = T_{nom} - (T_{nom} - T_{ini}) \exp(-\ln(2) t/t_{1/2}) \quad (4)$$

where  $T$  is the temperature growing from the room temperature  $T_{ini}$  to temperature  $T_{nom}$  and  $t_{1/2}$  is the heating time to temperature rise to  $(T_{nom}-T_{ini})/2$ . Here the value of  $t_{1/2}$  was assumed to be of about 15 s.

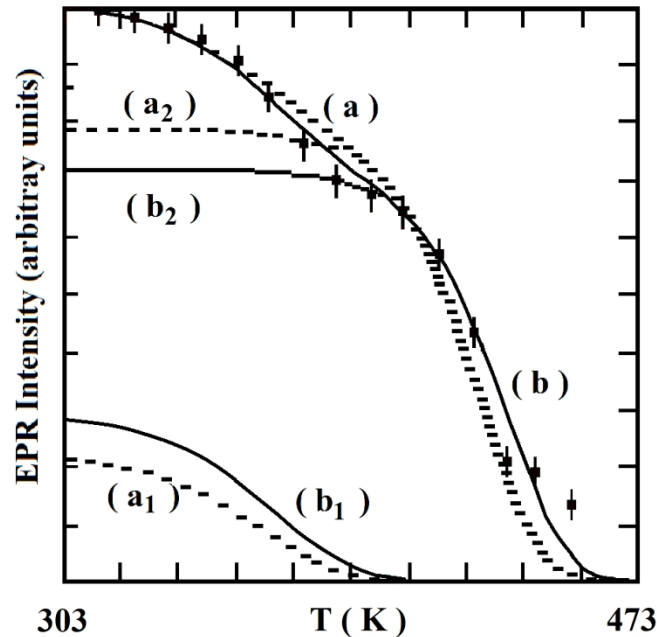


**Fig. 4. Isochronal decay of atomic hydrogen EPR absorption performed with temperature pulses. Dashed line (a) shows the result calculated using parameters obtained in the analysis of the isothermal decay and (a1) and (a2) the contributions from energies E1 and E2. Solid line (b) shows the best fit result and (b1 and (b2) the contributions from energies E1 and E2**

At first, we calculated the isochronal decay of  $H^0$  using the parameters obtained in the analysis of the isothermal decay. The result is shown as dashed lines in Fig. 4. We can observe that the calculated curve shown in Fig 4a as dashed line reproduces the order of magnitude of the experimental points. In Fig. 4a<sub>1</sub> and 4a<sub>2</sub> we show the contributions of the energies  $E_1$  and  $E_2$ , respectively. This observation reinforces the model of two independent center of  $H^0$  used in the analysis of isothermal decays.

However as the data obtained contains inaccuracies in the measurement of the absorption line intensity and determination of EPR annealing time a best fit was not performed because our software can not consider such inaccuracies. But, for illustration purposes, we made a rough fitting, the result of which we show in Fig. 4b as a continuous line, with the respective contributions of the energies  $E_1$  and  $E_2$  in the Fig. 4b<sub>1</sub> and Fig. 4b<sub>2</sub>. The fit was obtained with  $E_1 = 0.56$  eV and  $E_2 = 1.0$  eV, and pre-exponential factors  $b_{01} = 35.7 \cdot 10^3 \text{ s}^{-1}$  and  $b_{02} = 56.5 \cdot 10^7 \text{ s}^{-1}$ , respectively.

#### 4. CONCLUSION

The results of the present analysis show that the isothermal decays are made up of at least two exponential decays, indicating two simultaneous processes of first order decay. The parameters of the isochronal decay analysis presented good adherence to the measured data.

In barium aluminoborate glasses, the  $H^0$  is unstable at room temperature, since  $H^0$  is stabilized by van der Waals forces at the centers of oxygen polygons belonging to B–O ring structures in the glass network [4-6] with activation energies below 0.32 eV [6]. On the other hand, the activation energy 0.56 eV [19] of the  $H^0$  found in a:Si(H,O,N) is comparable to the first stabilization center of rubellite with activation energy 0.55 eV, both being stable above room temperature. This reinforces the model of cages formed laterally by a ring structure of six  $SiO_4$  tetrahedra, with brucite octahedra at the bottom and  $Y^+$  ( $Y=Na, K$ ) ions covering the top of the antigorite structure [1].

After  $H^0$  recombines it is impossible to further observe paramagnetic atomic hydrogen unless the sample is re-irradiated with a photolytic source. This means that thermal energy cannot produce  $H^0$  from the recombined hydrogen and we may easily rule out bond-breaking diffusion [20-24] or mediation by the dangling bond migration model [25,26] as the mechanism for the thermal decay of the neutral atomic hydrogen.

## ACKNOWLEDGEMENTS

This work was supported with grants from FAPESP, RHAЕ (SCT), FINEP and CNPq.

## COMPETING INTERESTS

Authors have declared that no competing interests exist.

## REFERENCES

1. de Camargo MB, Pontuschka WM, Isotani S. Electron paramagnetic resonance of atomic hydrogen centers in rubellite. *Anais da Academia Brasileira de Ciencias* 1987;59:293-298.
2. de Camargo MB. Ressonância paramagnética eletrônica de centros de hidrogênio atômico na turmalina rosa do Brasil, Doctoral Thesis, University of São Paulo; 1985.
3. de Camargo MB, Isotani S. Optical absorption spectroscopy of natural and irradiated pink tourmaline. *American Mineralogist* 1988;73:172-180.
4. Godovikov AA. *Mineralogy. Nedra. Moscow*; 1975.
5. Buerger MJ, Burnham CW, Peacor DR. Assessment of the several structures proposed for tourmaline. *Acta Crystallographica* 1962;15:583-590.
6. Pontuschka WM. Neutral atomic centers in amorphous systems. *Journal of Optoelectronics and Advanced Materials*. 2002;535-541.
7. Pontuschka WM, Isotani S, Piccini A, Vugman NV. EPR and kinetics studies of hydrogen centers in aluminoborate glasses. *J.Am.Ceramic. Soc.* 65, 1982;4:519-523.
8. Pontuschka WM, Isotani S. A model for the stabilization of atomic hydrogen centers in borate glasses. *Physica B: Condensed Matter*. 2009;404:4312-4315.
9. Alger RS. *Electron paramagnetic resonance-Techniques and applications*, John Wiley & Sons, New York; 1968.
10. Pake GE, Estle W. *The physical principles of electron paramagnetic resonance*, 2<sup>nd</sup> edition, *Frontiers in Physics*, Benjamin, New York; 1973.
11. Koryagin VF, Grechushnikov BN. Electron Paramagnetic resonance of atomic hydrogen in beryl. *Sov. Phys. Solid State*. 1966;7,8:2010-2012.
12. Isotani S, Albuquerque ARPL, Capeli OM. *IEEE International Conference on Systems, Man and Cybernetics, SMC'94, San Antonio, EUA*. 1994;254.

13. Isotani S, Fujii AT. A grid procedure applied to the determination of parameters of a kinetic process. Computer Physics Communications 2003;151:1-7.
14. Isotani S, Blak AR, Watanabe S. UV optical absorption spectra analysis of beryl crystals from Brazil. Physica B. 2010;405:1501-1508.
15. Isotani S, Matsuoka M, ARPL Albuquerque. Isothermal annealing of a 620 nm optical absorption band in Brazilian topaz crystals. Physica B. 2013;415:38-43.
16. Isotani S, Furtado WW, Antonini R, Blak AR, Pontuschka WM, Tome T, Rabbani SR. Decay kinetics study of atomic hydrogen in a-Si:(H,O,N) and natural beryl. Physical Review. 1990;B42:5966-5972.
17. Press WH, Flannery BP, Teukolsky SA, Vetterling WT. Numerical Recipes in C. The Art of Scientific Computation, Cambridge, New York; 1988.
18. Fujii AT, Isotani S. Thermal equilibrium times measurement. Semina. 1982;12:269-272. Portuguese.
19. Pontuschka WM, Carlos WW, Taylor PC, Griffith RW. Radiation induced paramagnetism in a:Si(H,O,N). Physical Review. 1982;B25:4362-4376.
20. Carlson DE, Magee CW. A SIMS analysis of deuterium diffusion in hydrogenated amorphous silicon. Appl. Phys. Lett. 1978;33:81-83.
21. Street RA, Tsai CC, Kakalios J, Jackson WB. Hydrogen diffusion in amorphous silicon. Philos. Mag. 1987;B56:305-320.
22. Kakalios J, Street RA. Thermal equilibrium processes in doped amorphous silicon. J. Non-Cryst. Solids 1987;97 & 98:767-774.
23. Jackson W, Tsai CC, Thompson R. Estimates of diffusion rate of the dominant paramagnetic defect in hydrogenated amorphous silicon, J. Non-Cryst. Solids. 1989;114:396-398.
24. Beyer W, Herion J, Wagner H. Fermi energy dependence of surface desorption and diffusion of hydrogen in a-Si:H. Non-Cryst. Solids. 1989;114: 217-219.
25. Pantelides ST. Defect dynamics and the Staebler-Wronski effect in hydrogenated amorphous silicon. Phys. Rev. 1987;B36:3479-3482.
26. Shinar R, Mitra S, Wu XL. J. Non-Cryst. Solids. 1989;114:220-222.

© 2014 Isotani and Pontuschka; This is an Open Access article distributed under the terms of the Creative Commons Attribution License (<http://creativecommons.org/licenses/by/3.0>), which permits unrestricted use, distribution, and reproduction in any medium, provided the original work is properly cited.

*Peer-review history:*

*The peer review history for this paper can be accessed here:*  
<http://www.sciencedomain.org/review-history.php?iid=283&id=4&aid=2205>